Journal of Catalysis 264 (2009) 117–129

Contents lists available at ScienceDirect

Journal of Catalysis

journal homepage: www.elsevier.com/locate/jcat

Kinetic and mechanistic studies of the water–gas shift reaction on Pt/TiO_2 catalyst

Christos M. Kalamaras [a], Paraskevi Panagiotopoulou [b], Dimitris I. Kondarides [b,*], Angelos M. Efstathiou [a,*]

[a] Department of Chemistry, Heterogeneous Catalysis Laboratory, University of Cyprus, P.O. Box 20537, CY 1678, Nicosia, Cyprus
[b] Department of Chemical Engineering, University of Patras, GR-26504 Patras, Greece

ARTICLE INFO

Article history:
Received 11 December 2008
Revised 3 March 2009
Accepted 10 March 2009
Available online 28 April 2009

Keywords:
Water–gas shift reaction
Platinum
TiO_2
Kinetic study
WGS reaction mechanism
SSITKA–DRIFTS
SSITKA–mass spectrometry
Operando studies
DRIFTS

ABSTRACT

A detailed kinetic and mechanistic study of the water–gas shift (WGS) reaction on a 0.5 wt% Pt/TiO_2 catalyst has been carried out. The dependence of kinetic reaction rate on the partial pressures of reactants (CO, H_2O) and products (H_2, CO_2), and the concentration and chemical structure of *active* and *inactive reaction intermediates* that are found in the "hydrogen-path" and "carbon-path" of the reaction have been investigated in the 200–270 °C range. The most likely mechanistic pathway of the WGS reaction over the present catalytic system is discussed. It has been found that the reaction rate increases with an increase in the concentration of CO or H_2O in the feed stream, while it decreases significantly with the addition of H_2 in the feed stream. On the contrary, the kinetic reaction rate was found to be practically independent on the concentration of CO_2 in the feed stream. The experimental reaction rates that were estimated were fitted to an empirical power-law rate expression from which the kinetic reaction orders with respect to CO, H_2O, CO_2, and H_2 were estimated to be 0.5, 1.0, ~0.0, and −0.7, respectively. An apparent activation energy of 10.8 kcal/mol was also estimated. The formation of formate and carbonate surface species over the TiO_2 support under WGS reaction conditions was proved via SSITKA–DRIFTS experiments. However, these reaction intermediates must be considered as *inactive* (spectator) species for the steady-state WGS reaction. Additional transient experiments that involved ^{18}O-isotope provided strong support for the *red-ox mechanism* as the prevailing one on the present Pt/TiO_2 catalyst, where labile oxygen and oxygen vacancies of TiO_2 near the metal–support interface can participate in the reaction path of the WGS reaction.

1. Introduction

The heterogeneously catalyzed water–gas shift (WGS) reaction

$$CO + H_2O \leftrightarrow CO_2 + H_2 \quad (\Delta H^0_{298\,K} = -41.1\ kJ/mol) \qquad (1)$$

has historically been an important industrial chemical process for the synthesis of ammonia, the hydro-processing of petroleum, the production of hydrogen via steam reforming of hydrocarbons [1], and in fuel cell applications for providing purification of CO and thus clean hydrogen supply [2,3]. The WGS reaction is moderately exothermic and equilibrium limited, and, therefore, low CO levels can only be achieved at low temperatures with favorable kinetics at higher temperatures.

It is generally accepted that the WGS reaction over metal oxide-supported noble metal catalysts operates in a bifunctional manner with the participation of both the dispersed metal and the support phases [4–6]. In this regard, two general mechanistic schemes have been proposed: (a) a red-ox or "regenerative" mechanism [7–10], according to which CO adsorbed on the metal phase is oxidized to CO_2 by labile oxygen of the support, the latter being re-oxidized by water, a reaction step that leads to the formation of hydrogen, and (b) an associative mechanism [11–13] according to which the reaction proceeds via the interaction of adsorbed CO with the terminal hydroxyl groups of the oxidic support to form a formate intermediate, which is further decomposed to CO_2 and H_2 gases.

Steady-state isotopic transient kinetic analysis (SSITKA) has long been documented and widely accepted as one of the most powerful techniques to elucidate the mechanisms of heterogeneous catalytic reactions in a rigorous manner [14]. For the present catalytic system, only a few studies dealing with the application of SSITKA technique were reported. The reverse WGS reaction in the absence of water over a Pt/CeO_2 catalyst was studied by Tibiletti et al. [15] and Goguet et al. [16] by SSITKA–DRIFTS. It was found that the main active reaction intermediate for the formation of CO was carbonate, and that surface formate (–COOH) would rather be considered as a spectator species. Jacobs et al. [17,18] investigated the low-temperature (225 °C) forward WGS reaction over the same catalyst by SSITKA–DRIFTS. The authors confirmed that formate is an active intermediate of the WGS reaction as opposed to the case of the reverse WGS reaction [15,16].

* Corresponding authors. Fax: +30 2610 991527 (D.I. Kondarides), +357 22 892801 (A.M. Efstathiou).
E-mail addresses: dimi@chemeng.upatras.gr (D.I. Kondarides), efstath@ucy.ac.cy (A.M. Efstathiou).

0021-9517/$ - see front matter © 2009 Elsevier Inc. All rights reserved.
doi:10.1016/j.jcat.2009.03.002

Recently, Azzam and co-workers [19,20] have used *in situ* FTIR and transient kinetic experiments to study the WGS reaction mechanism over supported Pt catalysts (CeO_2, ZrO_2 and TiO_2). They proposed that in the case of Pt/ZrO_2 the WGS reaction follows the associative formate route with red-ox regeneration, whereas in the case of Pt/TiO_2 both the red-ox and the associative formate routes with red-ox regeneration apply. On the contrary, the associative formate route is the relevant reaction pathway on Pt/CeO_2 [20].

In the present work, SSITKA–DRIFTS experiments have been performed to probe the *chemical structure* of *active* and *inactive* (spectator) reaction intermediates found in the carbon-path of the WGS reaction over a 0.5 wt% Pt/TiO_2 catalyst. The surface concentrations (μmol/g, θ) of active "H-containing" and "C-containing" surface reaction intermediates were measured by *in situ* SSITKA–mass spectrometry experiments. Specially designed $^{18}O/^{16}O$ isotopic exchange experiments followed by WGS reaction experiments were used to probe the red-ox mechanistic path with the participation of surface labile oxygen of the TiO_2 support in the overall WGS reaction mechanism.

The kinetics of the WGS reaction over supported noble metal catalysts as well as over the Cu- and Fe-based catalysts have been studied by several groups, and numerous kinetic models based either on the red-ox or on the associative mechanism have been proposed [11,21–23]. Furthermore, a number of empirical (power-law) rate expressions have been reported in order to obtain the orders of the WGS reaction with respect to the reactants and products based on intrinsic kinetic rate experimental data [1,8,21,24–28]. It is well known that it is difficult to determine the reaction mechanism based on steady-state kinetic rate data and an assumed sequence of elementary steps having also postulated one rate-determining step (reaction mechanism) since more than one mechanism can fit the same experimental data equally well and/or lead to the same overall kinetic rate expression. However, detailed kinetic results provide indications for the prevailing reaction mechanism, and sometimes specific mechanisms could be excluded. Moreover, a power-law rate expression is useful in reactor design calculations, where an accurate analytical expression of the reaction rate is required. Table 1 summarizes some of the empirical rate expressions (power-law) and reaction orders reported in the literature for supported metal catalysts [19,21,24,25,29,30].

In the present work besides the *in situ* mechanistic transient isotopic experiments performed as outlined above, a detailed kinetic study has also been carried out over the 0.5 wt% Pt/TiO_2 catalyst. This included the fitting of the experimental kinetic rate data to an empirical power-law expression, where the reaction orders with respect to reactants (CO and H_2O) and products (CO_2, H_2), and the apparent activation energy (E_{app}) of reaction were determined.

2. Experimental

2.1. Catalyst preparation and characterization

The Pt/TiO_2 catalyst was prepared employing the wet impregnation method by using TiO_2 (Degussa P25) carrier and $(NH_3)_2$-$Pt(NO_2)_2$ (Alfa) as a platinum precursor salt [5]. The Pt loading of the catalyst thus prepared was 0.5 wt%. The catalyst was characterized with respect to its specific surface area (BET, m^2/g), phase composition and crystallite size of the support, and exposed platinum surface area after employing N_2 physical adsorption (77 K), X-ray diffraction (XRD), and selective chemisorption of H_2 and CO, respectively, following the procedures described in detail elsewhere [5].

2.2. Kinetic measurements

Kinetic experiments have been carried out using the apparatus described in detail elsewhere [5]. It consists of a flow measuring and control system equipped with mass-flow controllers and a syringe pump, a quartz micro-reactor, and a gas chromatograph (Shimadzu) interfaced to a personal computer for *on-line* analysis of reactants and products. Reaction gases (He, 10%CO/He, H_2, and CO_2) of ultra-high purity were supplied from high-pressure gas cylinders (Messer Griesheim GMBH).

The effect of partial pressure of reactants (CO, H_2O) and products (H_2, CO_2) on the kinetic reaction rate has been investigated in the 210–270 °C range using a feed stream consisting of 0.05–9.0 vol% CO, 3.0–20.0 vol% H_2O, 0–18.0 vol% CO_2, and 0–50.0 vol% H_2 (balance He). Measurements of intrinsic kinetic rates were

Table 1
Summary of rate expressions (power-law) and reaction orders that appeared in the literature for the WGS reaction over different supported metal catalysts.

Catalyst	Power-law expression rate	References
Pd/CeO_2	$r = k \cdot P_{CO}^{a} \cdot P_{H_2O}^{b} \cdot P_{CO}^{c} \cdot P_{H_2}^{d}$ $a = 0$, $b = 0.5$, $c = -0.5$, $d = -1$	[25]
Rh/CeO_2	$r = k \cdot P_{CO}^{a} \cdot P_{H_2O}^{b}$ $a = 0$, $b = 1$	[24]
M/Al_2O_3	$r = k \cdot P_{CO}^{a} \cdot P_{H_2O}^{b}$	[21]
Ru	$a = -0.21$, $b = 0.66$	
Rh	$a = -0.10$, $b = 0.44$	
Pd	$a = 0.14$, $b = 0.38$	
Pt	$a = -0.21$, $b = 0.75$	
M/SiO_2	$r = k \cdot P_{CO}^{a} \cdot P_{H_2O}^{b}$	
Pt	$a = -0.08$, $b = 0.69$	
Rh	$a = -0.24$, $b = 0.53$	
Pt/CeO_2–ZrO_2	$r = A \cdot \exp\left(\frac{-E_a}{RT}\right) \cdot [CO]^{a} \cdot [H_2O]^{b} \cdot [CO_2]^{c} \cdot [H_2]^{d} \cdot (1-\beta)$ $a = 0.07$, $b = 0.67$, $c = -0.16$, $d = -0.57$, $E_a = 17$ kcal/mol, $A = 2.5 \cdot 10^7$	[30]
Pt–Re/CeO_2–ZrO_2	$r = A \cdot \exp\left(\frac{-E_a}{RT}\right) \cdot [CO]^{a} \cdot [H_2O]^{b} \cdot [CO_2]^{c} \cdot [H_2]^{d} \cdot (1-\beta)$ $a = -0.05$, $b = 0.85$, $c = -0.05$, $d = -0.32$, E_a=17 kcal/mol, $A = 4.5 \cdot 10^6$	[30]
Pt/Al_2O_3	$r = k_f \cdot [CO]^{a} \cdot [CO_2]^{b} \cdot [H_2]^{c} \cdot [H_2O]^{d} \cdot (1-\beta)$ $a = 0.1$, $b = -0.1$, $c = -0.5$, $d = 1.0$	[29]
Pt/CeO_2	$r = k_f \cdot [CO]^{a} \cdot [CO_2]^{b} \cdot [H_2]^{c} \cdot [H_2O]^{d} \cdot (1-\beta)$ $a = -0.03$, $b = -0.09$, $c = -0.38$, $d = 0.44$	[29]
Pt–Re/TiO_2	$r = k_f \cdot P_{CO}^{a} \cdot P_{H_2O}^{b} \cdot P_{H_2}^{c} \cdot P_{CO_2}^{d} \cdot (1-\beta)$ For high CO and low CO_2 concentrations: $a = 0.0$, $b = 0.8$, $c = -0.5$, $d = 0.0$ For high CO_2 and low CO concentrations: $a = 0.4$, $b = 0.7$, $c = -0.4$, $d = 0.0$	[19]

r: reaction rate, k: rate constant, P_i: partial pressure of species i, and β: the approach to equilibrium $\left(\beta = \frac{P_{CO_2} \cdot P_{H_2}}{K_{equil} P_{CO} \cdot P_{H_2O}}\right)$.

obtained under differential reaction conditions, where the conversion of reactant CO was typically kept below 10% by varying the mass of the catalyst (60–150 mg) and/or the total flow rate (100–300 N mL/min). Kinetic reaction rates were calculated using the following expression:

$$r_{CO} = \frac{\left(C_{CO}^{in} - C_{CO}^{out}\right)F}{W} \quad (2)$$

where r_{CO} is the conversion rate of CO (mol s^{-1} g_{cat}^{-1}), F is the total molar flow rate (mol/s) at the exit of the reactor, W is the mass of the catalyst (g), and C_{CO}^{in} and C_{CO}^{out} are the inlet and outlet concentrations (mol%) of CO, respectively. Details on the methods and procedures employed can be found elsewhere [5].

2.3. In situ DRIFTS – CO chemisorption studies

In situ DRIFTS studies were performed using a FTIR spectrometer (PerkinElmer Spectrum GXII) equipped with a temperature controllable DRIFTS cell (Harrick, Praying Mantis). In the case of CO/He and CO/H_2 adsorption studies, the catalyst sample in a very fine powder form was diluted with dry KBr (1:5 w/w) for improved signal-to-noise ratio. The spectrum of the solid catalyst taken under Ar flow at the desired reaction temperature following catalyst pre-treatment in 20% O_2/Ar at 500 °C for 2 h followed by H_2 (1 bar) at 300 °C for 2 h was subtracted from the spectrum of the catalyst obtained after exposure to the gas adsorption mixture. Signal averaging was set to 50 scans per spectrum, and the spectra were collected at the rate of 1 scan/s at a 2 cm^{-1} resolution in the 4000–800 cm^{-1} range. CO (0.5 vol% CO/He) and CO/H_2 (0.5 vol% CO/50 vol% H_2/He) chemisorptions were performed in the 25–250 °C range.

2.4. Mechanistic studies

2.4.1. SSITKA–mass spectrometry studies

The isotopes used in the steady-state isotopic transient kinetic analysis–mass spectrometry (SSITKA–MS) experiments were ^{13}CO (99.5 atom% ^{13}C, Spectra Gases) and deuterium oxide (D_2O) (99.96 atom% D, Aldrich). SSITKA experiments were performed using two HPLC pumps (GILSON 307) for the addition of H_2O and D_2O to the reactor feed stream in the Micro-reactivity Pro apparatus described in detail elsewhere [31]. SSITKA–MS experiments were performed in order to follow the "hydrogen-path" of the reaction and involved the switch 3%CO/10%H_2O/Ar/Kr (30 min, T) → 3%CO/10%D_2O/Ar (T, t) at T = 200 and 250 °C, while those performed to follow the "carbon-path" of the reaction involved the switch 3% ^{12}CO/10%H_2O/Ar/He (30 min, T) → 3%^{13}CO/10%H_2O/Ar (T, t). The dry gas from the exit of a condenser (Peltier system) placed downstream the reactor was directed to the mass spectrometer for *on line* recording of H_2, CO, and CO_2 normal and isotope-containing (D, ^{13}C) gaseous species [32]. It was estimated that the response time, τ, of this system (switching valve → micro-reactor → condenser → mass spectrometer) is about 10 s based on the transient response curve of Ar to the switch He → 1 vol% Ar/He [14].

Conversion of the D_2 response signal of the mass spectrometer to mole fraction (mol%) was made using a 5 mol%D_2/Ar (Spectra Gases) calibration gas mixture. The mass of Pt/TiO_2 catalyst was adjusted so as to keep the CO conversion below 20%. The total mass of the catalytic bed material was kept to 0.5 g (catalyst diluted with silica). Data acquisition with mass spectrometer was performed at a scan rate of 50 ms per cycle (five pre-selected appropriate mass numbers were used).

2.4.2. Operando SSITKA–DRIFTS–mass spectrometry studies

Operando studies were performed in a specially designed gas flow-system where the response time (τ) of the DRIFTS reactor cell (~30 mg Pt/TiO_2) which was estimated from the Ar transient response curve following the switch 10%H_2O/He → 10%H_2O/1%Ar/He (100 mL/min) was about 5 s [14,33]. A PerkinElmer FTIR spectrometer (Spectrum GX) equipped with a high-temperature/high-pressure temperature controllable DRIFTS cell (Harrick, Praying Mantis) with ZnSe windows was used for the *in situ* recording of IR spectra. Signal averaging was set to 50 scans per spectrum, and the spectra were collected at the rate of 0.2 scans/s (MCT detector) at a 2 cm^{-1} resolution in the 4000–500 cm^{-1} range. The collected DRIFTS spectra were smoothed in order to remove high-frequency noise, if necessary, and were further analyzed using the software Spectrum® (PerkinElmer) for Windows. Deconvolution of the thus derived DRIFTS spectra was performed according to the reported guidelines [34]. The background spectrum of the solid catalyst was taken under 10%H_2O/Ar flow (100 mL/min) at the desired reaction temperature. The IR data were reported as log1/R (absorbance mode) using the relationship $R = I/I_0$. Here, R is the catalyst sample reflectance, I_0 is the absorbance intensity of the solid catalyst itself, and I is the absorbance intensity of both the solid catalyst and adsorbate under reaction conditions. The function log1/R was found to give a better linear correlation of the infrared band area against surface concentration than that given by the Kubelka–Munk function for strongly absorbing media [35]. The noise level associated with the recorded infrared spectra in terms of absorbance units was estimated to be 0.0008.

SSITKA–DRIFTS experiments with ^{13}CO (99.5 atom% ^{13}C, Spectra Gases) which were performed using the DRIFTS reactor cell involved the switch 3%^{12}CO/10%H_2O/Ar/He (T, 30 min) → 3%^{13}CO/10%H_2O/Ar (T, t) at a total flow rate of 100 N mL/min in order to determine the chemical structure of the *active* and *inactive* (*spectator*) "carbon-containing" reaction intermediates of the WGS reaction. The product gas from the exit of DRIFTS cell was directed to the mass spectrometer (Balzer, Omnistar, 1–300 amu) for recording the *transient evolution* of gaseous H_2, He, CO, and CO_2 (normal and isotope-containing ^{13}C) species (*operando* studies).

2.4.3. $^{18}O/^{16}O$ isotope exchange experiments followed by WGS reaction

$^{18}O/^{16}O$ isotopic exchange experiments were carried out in the same apparatus that was used for conducting the SSITKA–mass spectrometry experiments (see Section 2.4.1). The catalyst sample (0.3 g) was placed in a quartz micro-reactor, and was first pre-treated with 5%$^{18}O_2$/He (97% ^{18}O atoms, Marshall isotopes Ltd) at 600 °C for 30 min, and then reduced under hydrogen (1 bar) at 80 °C for 20 min. The $^{18}O/^{16}O$ isotopic exchange was monitored with an *on-line* mass spectrometer by recording the evolution of $^{16}O_2$, $^{16}O^{18}O$, and $^{18}O_2$ gaseous species (m/z = 32, 34, and 36). Following the H_2 gas treatment, the sample was heated from 80 to 200 °C in He flow and was then exposed to the WGS reaction feed stream (3 vol% CO/10 vol% H_2O/Ar) at a total flow rate of 200 N mL/min. The mass numbers (m/z) 2 (H_2), 28 ($C^{16}O$), 44 ($C^{16}O_2$), 46 ($C^{16}O^{18}O$), and 48 ($C^{18}O_2$) were continuously monitored by mass spectrometry. In another experiment that probed the isotopic exchange of pre-adsorbed ^{18}O on the catalyst surface with $C^{16}O_2$(g), following the $^{18}O_2$/He and H_2 gas treatments described above, the gas flow was switched to a 0.3 vol% $C^{16}O_2$/Ar gas mixture at 200 °C, and all the isotopic carbon dioxide species that formed were recorded with an on-line mass spectrometer.

3. Results

3.1. Catalyst characterization

Results of catalyst characterization showed that the specific surface area (BET) of the 0.5 wt% Pt/TiO_2 catalyst was 41 m^2/g,

whereas the Pt dispersion was 87%. The TiO_2 support consists of 75% anatase with a primary crystallite size of 25 nm [4].

3.2. Kinetic measurements on 0.5 wt% Pt/TiO_2 catalyst

The effect of partial pressures of reactants (CO, H_2O) and products (H_2, CO_2) on the kinetic rate of WGS reaction has been investigated in the 210–270 °C range. Fig. 1A shows the dependence of the intrinsic reaction rate (mol/g s) on the partial pressure of CO, where H_2O, CO_2, and H_2 partial pressures were kept constant at the values of 0.10, 0.06, and 0.20 atm, respectively. It is observed that by increasing the partial pressure of CO from 0.005 to 0.06 atm the reaction rate increases by about a factor of three for all the temperatures examined. The effect of H_2O partial pressure on the reaction rate was studied at 230 and 250 °C where it was found that the reaction rate increases by about a factor of four with an increase of P_{H_2O} from 0.06 to 0.19 atm (Fig. 1B).

Similar kinetic experiments were conducted by varying the concentration of CO_2 and H_2 in the feed composition as depicted in Fig. 2. It was found that the reaction rate is not practically affected by increasing the partial pressure of CO_2 at least in the range of 0–0.18 atm (Fig. 2A). In contrast, addition of H_2 in the feed gas mixture even at a very low concentration (0.5 vol%) led to a significant decrease (about one order of magnitude) in the WGS reaction rate (Fig. 2B). However, for higher partial pressures of H_2 (0.1–0.5 atm) the negative effect of P_{H_2} on the reaction rate is much less pronounced (Fig. 2B).

The orders of the WGS reaction with respect to reactants and products for the present 0.5 wt% Pt/TiO_2 catalyst were determined by fitting the experimental data (Figs. 1 and 2) to an empirical power-law rate expression according to which the reaction rate is given by the following relationships:

$$r = k \cdot P_{CO}^{a} \cdot P_{H_2O}^{b} \cdot P_{CO_2}^{c} \cdot P_{H_2}^{d} \cdot (1-\beta) \quad (3)$$

$$k = k_0 \cdot e^{-E_a/R\cdot T} \quad (4)$$

where r is the reaction kinetic rate (mol s^{-1} g_{cat}^{-1}); k is the rate constant; P_i is the partial pressure of species i (atm); a, b, c, and d are the reaction orders with respect to CO, H_2O, CO_2, and H_2, respectively; β $\left(\beta = \frac{P_{CO_2}\cdot P_{H_2}}{K_{equil}\cdot P_{CO}\cdot P_{H_2O}}\right)$ is the approach to equilibrium; k_0 is the pre-exponential factor; E_a is the apparent activation energy of reaction (kcal/mol); R is the universal gas constant (cal/mol K); and T is the reaction temperature (K). It should be noted that the values of β in the present experiments were typically of the order of 0.0–0.15 which indicates that the WGS reaction was carried out far from equilibrium. Fitting of the experimental data to the power-law rate expression and determination of the kinetic parameters were carried out using the Sigma-Plot 8.0 program. The results that were

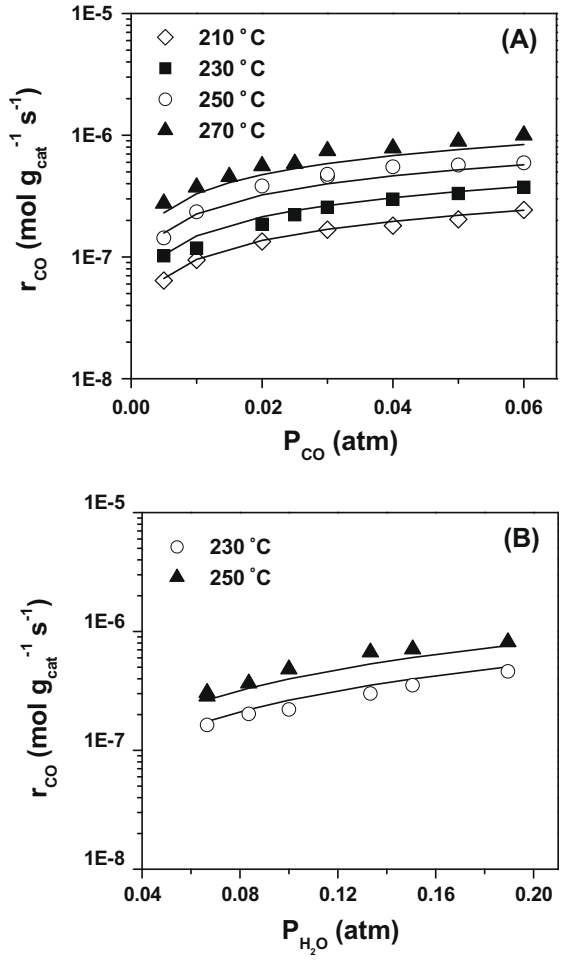

Fig. 1. (A) Effect of CO partial pressure on the kinetic reaction rate obtained in the 210–270 °C range for H_2O, CO_2, and H_2 partial pressures of 0.10, 0.06, and 0.20 atm, respectively. (B) Effect of H_2O partial pressure on the kinetic reaction rate at 230 and 250 °C, for CO, CO_2, and H_2 partial pressures of 0.03, 0.06, and 0.20 atm, respectively. The symbols correspond to the experimental data, whereas the lines represent the fitting of the kinetic rate expression (Eq. (5)) to the experimental data.

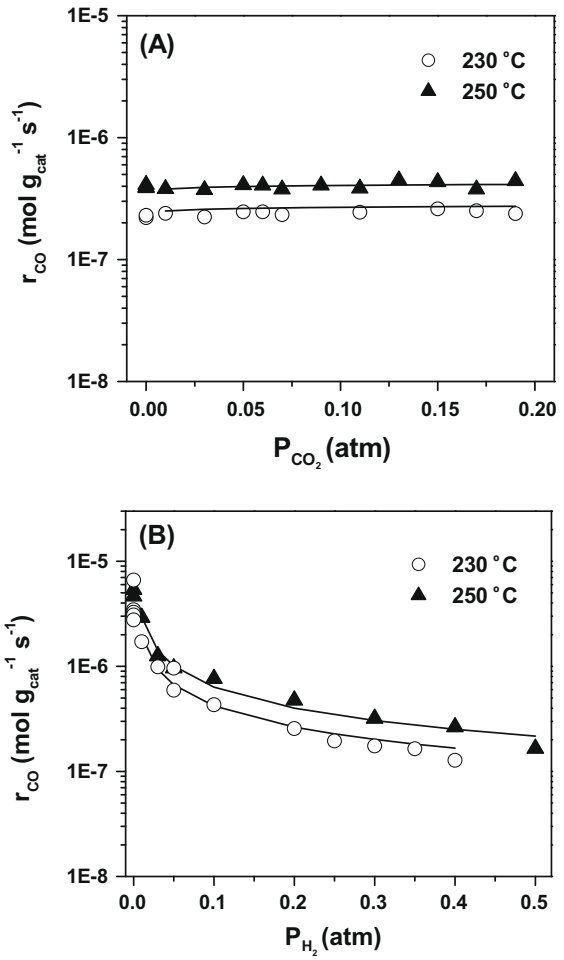

Fig. 2. (A) Effect of CO_2 partial pressure on the kinetic reaction rate at 230 and 250 °C, for CO, H_2O, and H_2 partial pressures of 0.03, 0.10, and 0.20 atm, respectively. (B) Effect of H_2 partial pressure on the kinetic reaction rate at 230 and 250 °C, for CO, H_2O, and CO_2 partial pressures of 0.03, 0.10, and 0.06 atm, respectively. The symbols correspond to the experimental data, whereas the lines represent the fitting of the kinetic rate expression (Eq. (5)) to the experimental data.

Table 2
Reaction orders, apparent activation energy, and pre-exponential factor for the WGS reaction which were obtained from the fitting of the empirical rate expression $r = k_0 \cdot e^{-E_a/R\cdot T} \cdot P_{CO}^{a} \cdot P_{H_2}^{b} \cdot P_{CO_2}^{c} \cdot P_{H_2}^{d} (1-\beta)$ to the experimental data. Feed composition: 0.05–9 vol% CO, 3–20 vol% H_2O, 0–50 vol% H_2, 0–18 vol% CO_2, He balance.

Catalyst	*a*	*b*	*c*	*d*	k_0	E_{app} (kcal/mol)
0.5% Pt/TiO_2	0.5	1.0	0.0	−0.7	0.31	10.8

obtained are summarized in Table 2. It is observed that reaction orders of 0.5 for CO, 1.0 for H_2O, zero for CO_2, and −0.7 for H_2 are obtained. The apparent activation energy was calculated to be 10.8 kcal/mol. After using the results reported in Table 2, and the experimental values of reaction rate versus P_i, optimum curves shown as solid lines in Figs. 1 and 2 were obtained.

The power-law rate expression (Eq. (3)) for a given feed gas composition can be expressed as a function of reaction temperature, according to the following relationships:

$$r = k_0 \cdot e^{-E_a/R\cdot T} \cdot P_{CO}^{a} \cdot P_{H_2O}^{b} \cdot P_{CO_2}^{c} \cdot P_{H_2}^{d} \quad (5)$$

or

$$r = 0.31 \cdot e^{-10.8/R\cdot T} \cdot P_{CO}^{0.5} \cdot P_{H_2O}^{1} \cdot P_{CO_2}^{0} \cdot P_{H_2}^{-0.7} \quad (6)$$

The Arrhenius-type diagram shown in Fig. 3 illustrates the fitting of reaction kinetic rate measurements to Eq. (6) obtained for four different feed compositions. Clearly, the prediction of the power-law rate expression is in reasonable agreement with the experimental kinetic measurements.

Fig. 4 compares the kinetic reaction rates measured experimentally against those predicted according to the power-law rate expression for all feed compositions and reaction temperatures investigated. The comparison was carried out in the 200–420 °C range using 90 experimental data points. It is evident that a straight line fits the experimental results very well, thus enhancing the credibility of the proposed rate equation.

In order to obtain fundamental insight on the negative reaction order with respect to hydrogen (Fig. 2B), *in situ* DRIFTS spectra in the 2150–1650 cm^{-1} range recorded after CO chemisorption and CO/H_2 co-adsorption at 200 °C for 20 min over the 0.5 wt% Pt/TiO_2 catalyst are presented in Fig. 5a. It is observed that under the CO/He adsorption mixture (solid line, Fig. 5a) the spectrum is characterized by three IR bands in the ν(CO) region, centered at 2060, 1985, and 1760 cm^{-1}. The IR bands at 2060 and 1760 cm^{-1} are characteristic of linear- and bridge-bonded CO, respectively,

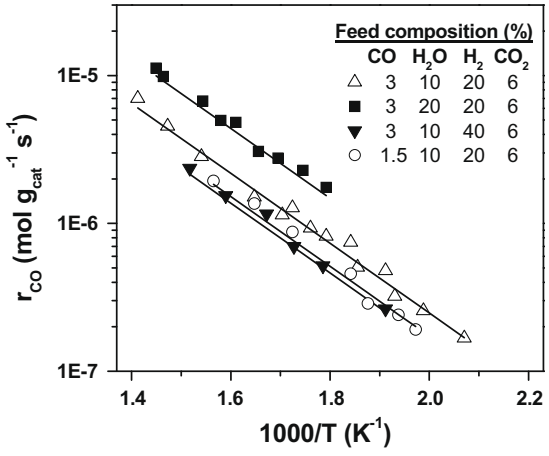

Fig. 3. Arrhenius plots of kinetic reaction rates obtained under the indicated feed compositions. The symbols correspond to the experimental data, whereas the lines represent the fitting of the kinetic rate expression (Eq. (5)) to the experimental data.

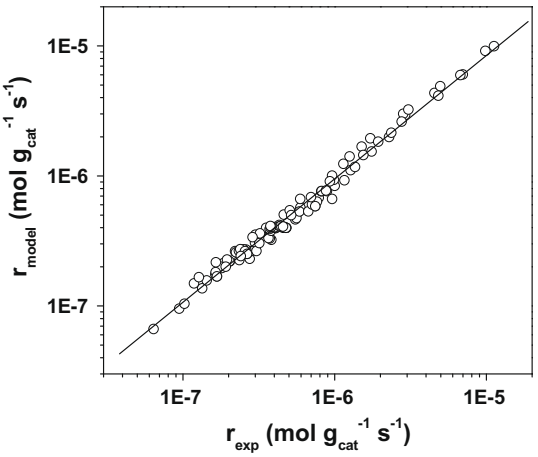

Fig. 4. Comparison between the experimentally measured kinetic reaction rates and those predicted from the power-law rate expression (Eq. (5)).

on the surface of reduced Pt crystallites [4,36–41]. The low-frequency (LF) IR band centered at 1985 cm^{-1} can be attributed to linear CO adsorbed either on isolated Pt sites or, most likely, on Pt sites of exceptionally high electron-donating properties [4,36–41]. Similar IR bands in the 1940–1980 cm^{-1} region have been reported for a number of noble metal catalysts dispersed on reducible supports, including Pt/TiO_2 [4,36,37], Au/TiO_2 [38], Pt/CeO_2 [39,40], and Pd/CeO_2 [41]. As discussed in detail in previous studies [4,36], IR bands in this frequency region could be assigned to linear CO adsorbed on Pt adjacent to reduced titania sites [Pt-$\square_s$-Ti^{3+}] at the metal–support interface.

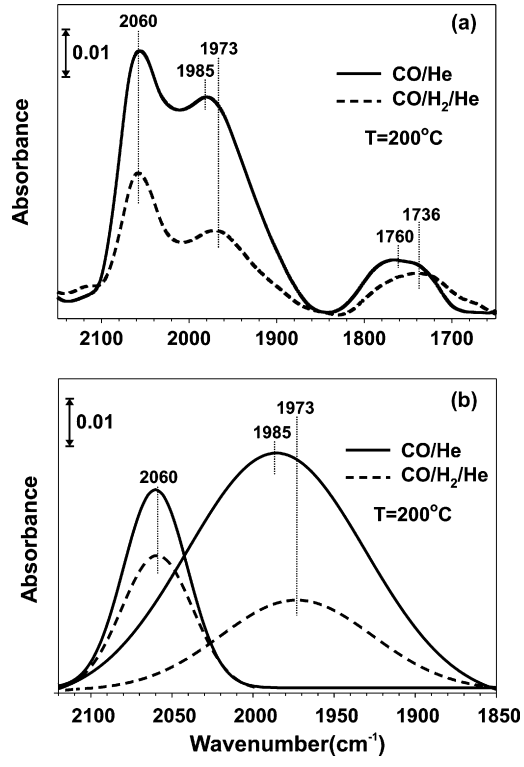

Fig. 5. (a) *In situ* DRIFTS spectra recorded in the 2150–1650 cm^{-1} range after 20 min of CO chemisorption (solid line spectrum) and CO/H_2 co-adsorption (dashed line spectrum) experiments at 200 °C over the 0.5 wt% Pt/TiO_2 catalyst. (b) Deconvolution and curve fitting of the infrared band 2100–1850 cm^{-1} due to linear adsorbed CO species recorded under CO chemisorption (solid line IR bands) and CO/H_2 co-adsorption (dashed line IR bands) according to (a).

Similar qualitative results were obtained in the case of CO/H_2 co-adsorption (dashed line, Fig. 5a), but the surface concentration of adsorbed CO was significantly reduced compared to CO chemisorption alone, as evidenced after comparing the corresponding integral area bands. Furthermore, the LF-linear CO band (1985 cm^{-1}) shifts toward lower wave numbers in the presence of H_2 (1973 cm^{-1}), which is not the case for the 2060 cm^{-1} IR band (CO adsorbed on the surface of Pt crystallites). To exclude the possibility that the shift of the 1985 cm^{-1} IR band is due to the overlapping of the two linear CO IR bands of different intensities, deconvolution of the 2100–1850 cm^{-1}IR band was performed and the results that were obtained are presented in Fig. 5b. It is clearly seen that the observed red shift in the LF-linear CO is not due to the above-mentioned reasons, but is due to other intrinsic ones. It is known that the decrease in the surface coverage of adsorbed CO results in a decrease in the induced dipole–dipole interactions between adjacent adsorbed CO species, thus an increase in the binding energy of adsorbed CO is obtained. This in turn would result in a shift in the IR band of adsorbed CO to lower wave numbers [42]. In the present work (Fig. 5a), a strong shift in the appearance of bridged CO (1760 cm^{-1}) was seen, where the surface coverage remained practically the same under the two gas atmospheres. On the other hand, in the case of high-frequency linear CO (2060 cm^{-1}) even though its coverage was reduced by about 30% (Fig. 5b), no shift in the corresponding IR band was seen. Therefore, as mentioned in the previous paragraph, it is suggested that the LF-linear CO (1985 cm^{-1}, Fig. 5a) is likely to be associated with the reduced titania sites [Pt-$\square_s$-Ti^{3+}] at the metal–support interface, where its bonding strength is also determined by the charge transfer between Pt and TiO_2. It is interesting to note that the presence of H_2 in the CO/H_2/He gas adsorption mixture has doubled the ratio of the surface concentrations of CO_{L1} (2060 cm^{-1}) to CO_{L2} (1985 or 1973 cm^{-1}) with respect to the CO/He gas adsorption mixture (ca. 0.6 vs. 0.3), thus affecting the LF-linear CO more.

Regarding the extent of electronic interaction between Pt and TiO_2, it is well known that noble metals (including Pt) do not interact strongly with stoichiometric TiO_2 [43]. However, results of XPS and UPS experiments performed on Pt/TiO_2(110) show that a localized electronic charge transfer occurs from Ti^{3+} states to Pt clusters in the presence of surface defects [44]. Thus, partial reduction of the titania surface under CO/H_2 atmosphere is expected to result in the creation of a higher amount of surface defects in the neighborhood of the dispersed metal crystallites, and, therefore, in the enhancement of charge transfer to dispersed Pt. This, in turn, should result in a decrease of the C–O bond strength of adsorbed CO at the metal–support interface, and in a shift of the corresponding infrared band toward lower wave numbers in agreement with the present results shown in Fig. 5.

3.3. Mechanistic studies on 0.5 wt% Pt/TiO_2 catalyst

3.3.1. SSITKA–mass spectrometry

Steady-state isotopic transient kinetic analysis (SSITKA) experiments were performed to follow the hydrogen-path ("H-path") of the WGS reaction mechanism from H_2O to the H_2 product gas under kinetic regime conditions (X_{CO} < 20%), following the switch 3%CO/10%H_2O/Ar/Kr (30 min, T) → 3%CO/10%D_2O/Ar (T, t) at 200 and 250 °C. Fig. 6A presents transient concentration response curves of H_2, HD, D_2, and Kr gases which were obtained after the isotopic switch was made over the Pt/TiO_2 catalyst at 200 °C. The amount of active "H-containing" intermediate species ("H-pool") that are found in the "H-path" of the WGS reaction is estimated based on the transient response curves of H_2, HD, and Kr, details of which were previously reported [14,32,33].

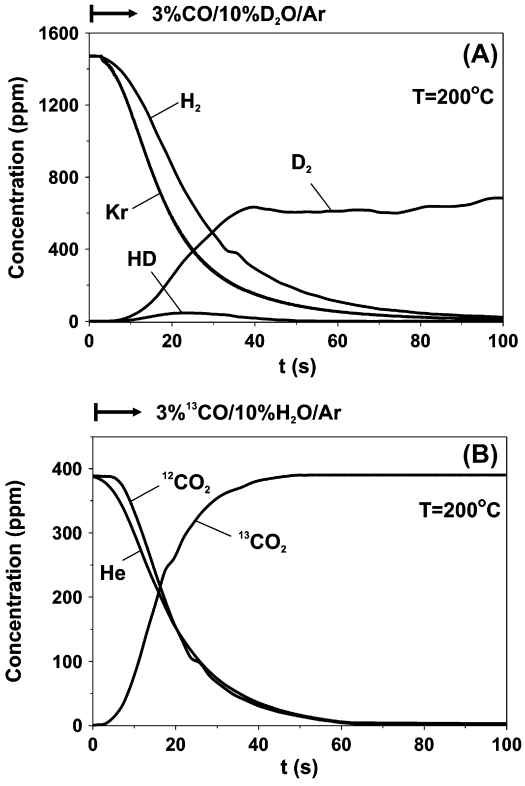

Fig. 6. SSITKA–mass spectrometry experiments performed to quantify the "H-path" (A) and "C-path" (B) of the WGS reaction at 200 °C on the 0.5 wt% Pt/TiO_2 catalyst. Gas delivery sequence: (A) 3%CO/10% H_2O/Ar/Kr (30 min) → 3%CO/10% D_2O/Ar (t); (B) 3%^{12}CO/10% H_2O/Ar/He (30 min) → 3%^{13}CO/10% H_2O/Ar (t). The mass of Pt/TiO_2 catalyst that was used was 0.3 g in (A) ($X_{CO} \sim 18\%$) and 0.1 g in (B) ($X_{CO} \sim 5\%$).

The SSITKA switch 3%^{12}CO/10%H_2O/Ar/He (30 min, T) → 3%^{13}CO/10%H_2O/Ar (T, t) at 200 and 250 °C was performed for the measurement of the concentration of active "carbon-containing" intermediate species, "C-pool". The dynamic responses of $^{12}CO_2$, $^{13}CO_2$, and He which were obtained upon the isotopic switch at 200 °C are presented in Fig. 6B. The concentration (μmol/g) of "C-pool" participating in the "carbon-path" of the WGS reaction from CO to the CO_2 reaction product can be estimated based on the transient response curves of $^{12}CO_2$ and He and an appropriate material balance equation [33].

The concentration of the "H-pool" was found to be 39.3 ± 3 μmol H/g or 1.75 ± 0.15 equivalent monolayers of surface Pt (θ_H = 1.75), and 112 ± 8 μmol H/g (θ_H = 5.0) at 200 and 250 °C, respectively. Similarly, the concentration of the "C-pool" was found to be 1.6 ± 0.15 μmol C/g (θ_C = 0.007) at 200 °C, and 3.9 ± 0.2 μmol C/g (θ_C = 0.18) at 250 °C. Details of the proper experimental precautions that are to be taken for the accurate performance of the SSITKA technique and the recording of transient response curves were reported [14,32,33].

In the SSITKA experiment, the evolution of the product formation response, for example, of $^{12}CO_2$(g) and $^{13}CO_2$(g) shown in Fig. 6B will be influenced if CO_2 interacts reversibly with the catalyst surface. If this is the case, it is implied that under steady-state WGS reaction conditions there is a pool of adsorbed CO_2 through which "^{13}C" must pass through, and a time constant must be associated with this pool. The amount of adsorbed CO_2 is therefore included in the value of "C-pool" reported in the previous paragraph. Based on this remark the concentration of active "carbon-containing" reaction intermediates must be even lower than what is stated above. According to the SSITKA–DRIFTS work to be presented next, the concentration of reversibly adsorbed carbonate species, if any,

is very small (not detectable by isotopic exchange). In the case of "H-pool" (Fig. 6A), any reversibly adsorbed H or D on the Pt surface is included in the estimation of the amount of "H-pool" given previously. However, since H_2(g) on Pt is expected to be formed by the recombination of two adjacent H adsorbed species, the adsorbed H on Pt is a true active reaction intermediate species.

3.3.2. Operando SSITKA–DRIFTS–mass spectrometry studies

In situ DRIFTS spectra recorded in the 3000–1300 cm^{-1} range on the 0.5 wt% Pt/TiO_2 catalyst during *operando* SSITKA–DRIFTS–mass spectrometry studies (see Section 2.4.2) at 200 °C are presented in Fig. 7A–C. The 1650–1300 cm^{-1} range (Fig. 7A) corresponds to the O–C–O stretching vibrational mode of formate, carbonate, and carboxylate species, that of 3000–2800 cm^{-1} (Fig. 7B) corresponds to formate (COOH) species (νCH and δCH + νOCO_a vibrational modes) [12,13,45–47], whereas the 2100–1850 cm^{-1} range (Fig. 7C) corresponds to linear adsorbed CO [36–41,48–50]. The various infrared bands shown in Fig. 7A–C under the $^{12}CO/H_2O$ (solid line spectra) and $^{13}CO/H_2O$ (dashed line spectra) reaction mixtures were recorded after a steady state was achieved (30 min on reaction stream).

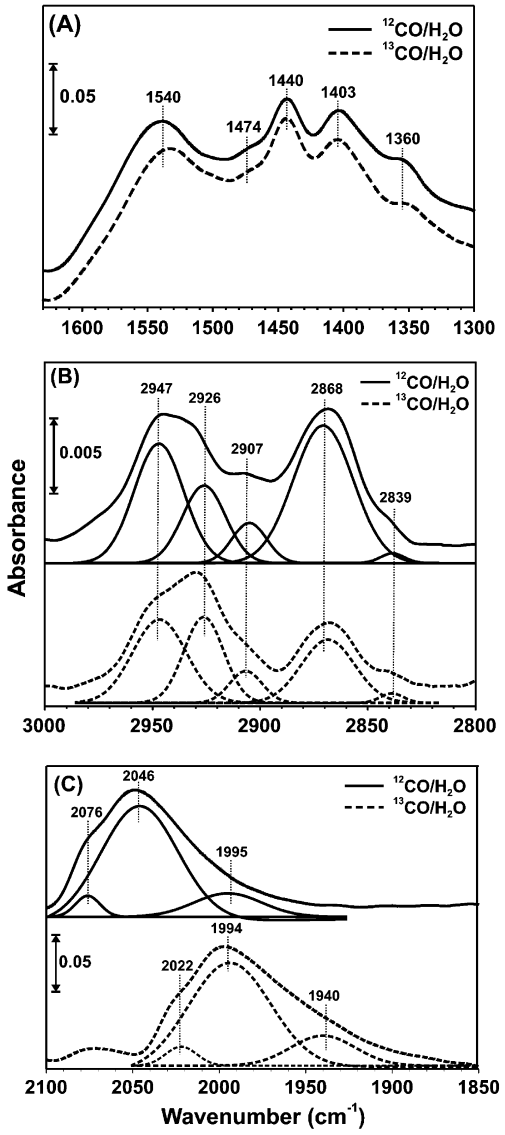

Fig. 7. DRIFTS spectra recorded in the 1650–1300 cm^{-1} (A), 3000–2800 cm^{-1} (B), and 2100–1850 cm^{-1} (C) ranges under steady-state WGS reaction conditions using 3%^{12}CO/10%H_2O/Ar/He (solid line spectra) and 3%^{13}CO/10%H_2O/Ar (dashed line spectra) feed gas compositions. In Figs. (B) and (C) deconvoluted DRIFTS spectra are also reported.

The broad IR band recorded in the 1600–1500 cm^{-1} range, and the IR band located at 1360 cm^{-1} (Fig. 7A) could potentially be assigned to the OCO_{as} vibrational mode of both formate and unidentate carbonate species. The IR band located at 1474 cm^{-1} corresponds to bidentate carbonate species, whereas the IR bands centered at 1440 and 1403 cm^{-1} correspond to bicarbonate-type chemisorbed carbon dioxide [12,13,45–47]. As depicted in Fig. 7A, none of the observed IR bands gave the expected red isotopic shift upon replacing the ^{12}C with ^{13}C in the "carbon-path" of the WGS reaction. Deconvolution and curve fitting of the spectra shown in Fig. 7A with five single peaks (Gaussian shape) centered at the indicated positions did not reveal any red shift within the experimental and analysis errors.

Five characteristic IR bands (2947, 2926, 2907, 2868, and 2839 cm^{-1}) due to νCH and δCH + νOCO_a vibrational modes of formate species that formed on the TiO_2 surface [32,33,45,46] were observed under $^{12}CO/H_2O$ and $^{13}CO/H_2O$ feed streams under steady-state reaction conditions at 200 °C as depicted in Fig. 7B. These IR bands are assigned to *two different kinds* of formate species, e.g. bidentate and bridged formate, or to the same formate structure coordinated to Ti–O–Ti moieties of different local chemical environments. It is noted that a sixth very small IR band centered at 2735 cm^{-1} (not shown in Fig. 7B) due to ν_s(OCO) + δ(CH) [51] was observed, thus fully justifying the presence of two kinds of adsorbed formate species on the titania surface. It is also mentioned here that adsorption of HCOOH(g) (use of 0.5 vol% HCOOH/Ar gas mixture) on the same Pt/TiO_2 catalyst placed in the DRIFTS cell resulted in IR bands that were almost identical in position to those shown in Fig. 7B. After deconvolution and curve fitting of the spectra shown in Fig. 7B under both $^{12}CO/H_2O$ and $^{13}CO/H_2O$ reaction feed streams, no measurable (larger than 2–3 cm^{-1}) isotopic shift in any of the five IR bands was detected. A noticeable small change by 0.001–0.003 Abs units in the intensities of the five deconvoluted IR bands shown in Fig. 7B obtained under the non-isotopic versus the isotopic reaction feed stream is considered within the error of the analyses procedure and the small change in the absorbance of the solid itself (background subtraction) which could have occurred within the 2-h interval time of the experimentation performed.

The most intense IR band recorded at 2046 cm^{-1} under the $^{12}CO/H_2O$ reaction mixture (Fig. 7C, solid line spectrum) corresponds to linear adsorbed CO [4,36–41,48–50]. After the new steady state in the rate of reaction under the isotopic gas mixture $^{13}CO/H_2O$ was reached, it is clearly seen that the IR band due to linear adsorbed CO gave the red isotopic shift (Fig. 7C, dashed line spectrum) with the new band centered at 1994 cm^{-1} ($\Delta\nu$ = 52 cm^{-1}). The small IR band centered at 2072 cm^{-1} and recorded under the $^{13}CO/H_2O$ gas treatment of the catalyst also gave the red isotopic shift (not shown under the $^{12}CO/H_2O$ mixture) and it was due to gaseous CO. Deconvolution and curve fitting ($R^2 > 0.985$) of the IR band recorded in the 2100–1850 cm^{-1} range (Fig. 7C) result in two other linear adsorbed CO species; a high-frequency linear CO (2076 → 2022 cm^{-1}) and a low-frequency linear CO (1995 → 1940 cm^{-1}) in addition to the most intense linear CO (2046 → 1994 cm^{-1}) that was observed.

The high-frequency linear CO (2076 cm^{-1}) can be assigned to CO adsorbed on the surface of Pt crystallites. In particular, the IR bands recorded at 2076 and 2046 cm^{-1} (Fig. 7C) were attributed to linear CO adsorbed on Pt terrace and step sites, respectively [36,52,53]. These IR bands can be clearly distinguished in the infrared spectra that were obtained following adsorption of CO on Pt/TiO_2 at room temperature. However, these infrared bands merge into a single IR band with an increase in the temperature (above

200 °C) [36]. This explains the appearance of a single IR band in this region in the spectrum presented in Fig. 5 (CO/He treatment). It is also important to note that the LF-linear CO (1995 → 1940 cm^{-1}) is formed under the WGS reaction conditions at 200 °C (Fig. 7C) as it was the case also under the CO/He gas treatment of the catalyst (Fig. 5a, 1985 cm^{-1}).

On the other hand, a very small IR band (∼ four times lower in intensity than the IR band at 1995 cm^{-1}) was recorded in the 1850–1700 cm^{-1} region due to bridged CO, as opposed to the case of CO/He adsorption (Fig. 5a). This means that either the bridged-CO is a very active reaction intermediate, or under the present WGS reaction conditions it is hardly populated on the Pt surface.

Fig. 8 shows the dimensionless concentration response curves (Z) of $^{12}CO(g)$, $^{12}CO_L(s)$, and $^{12}CO_2(g)$ "carbon-containing" species as a function of reaction time recorded under the isotopic switch 3%^{12}CO/10%H_2O/Ar/He (200 °C, 30 min) → 3%^{13}CO/10%H_2O/Ar (200 °C, t). The Z-$^{12}CO_L(s)$ response curve was estimated from the DRIFTS spectra that were collected every 20 s (use of MCT detector) based on the 2046 cm^{-1} IR band (linear CO) at maximum intensity which was recorded under the $^{13}CO/H_2O$ reaction mixture (Fig. 7C), and also according to the relationship reported elsewhere [33]. The gaseous transient response curves of $^{12}CO(g)$, $^{12}CO_2(g)$, and He were recorded simultaneously with an *on-line* mass spectrometer (see Section 2.4.2). As observed in Fig. 8, the $^{12}CO(g)$ response curve lags behind the He curve, where the concentration of $^{12}CO(g)$ practically goes to zero after 60 s of the isotopic switch. The area difference between the $^{12}CO(g)$ and He (tracer) transient response curves indicates that there must exist some reversibly adsorbed ^{12}CO that exchanges with $^{13}CO(g)$ which may or may not be a true active reaction intermediate species. Also, the possibility of having a "carbon-containing" intermediate species that is formed by a reversible interaction with CO(g) cannot be excluded, and this possibility is discussed later on. Based on these remarks, an upper limit for the concentration of "reversibly adsorbed CO" can be estimated from the $^{12}CO(g)$ and He responses (Fig. 8). This is found to be 22.0 μmol/g or $\theta = 0.95$ (based on surface Pt, 23.0 μmol/g) at 200 °C. The SSITKA–DRIFTS presented in Fig. 7C cannot provide a definite answer whether this reversible adsorbed CO does participate or not in the "C-path" of the WGS reaction since in both cases the red isotopic shift must be observed (Fig. 7C).

The growth of the transient evolution of $^{13}CO_2(g)$ reaction product is also presented in Fig. 8. The position of this transient response curve in time must be such that at every moment of the transient (under the $^{13}CO/H_2O$ switch) the sum of the concentrations of $^{12}CO_2$ and $^{13}CO_2$ must be equal to the steady-state concentration value of $^{12}CO_2$ obtained under the $^{12}CO/H_2O$ treatment. This means that in terms of the dimensionless concentration Z (Fig. 8) the sum of $Z(^{12}CO_2)$ and $Z(^{13}CO_2)$ must be equal to 1.0 at any time of the transient. The latter important criterion of the SSITKA experiment was satisfied within better than 8% in the present work (Fig. 8). In particular, it is noted that the two transient response curves cross each other at $Z = 0.485$ instead of at 0.5 (3% experimental error).

3.3.3. $^{18}O/^{16}O$ isotope exchange experiments followed by WGS reaction

The possible contribution of labile oxygen of TiO_2 support during the WGS reaction on the 0.5 wt% Pt/TiO_2 catalyst was probed by the isotopic experiment described in Section 2.4.3. Fig. 9a presents transient response curves of H_2, $C^{16}O_2$, $C^{16}O^{18}O$, and $C^{18}O_2$ obtained under the 3%CO/10%H_2O/He gas mixture according to the following sequence of catalyst gas treatment: 5%$^{18}O_2$/He (30 min, 600 °C) → He, cool down to 80 °C → 1 atm H_2 (20 min, 80 °C) → He (20 min, 200 °C) → 3%CO/10%H_2O/He (t, 200 °C). The amount (μmol/g) of isotopic $C^{18}O^{16}O$ and $C^{18}O_2$ species formed during the latter switch contains part of ^{18}O present on the titania support before the switch to the WGS reaction feed stream, and which likely participate in the "carbon-path" of the reaction.

In order to investigate the possibility that the $C^{18}O^{16}O$ and $C^{18}O_2$ transient responses shown in Fig. 9a are not the result of isotopic exchange of the produced $C^{16}O_2$ (WGS reaction) and pre-adsorbed ^{18}O on the titania surface, the following experiment was

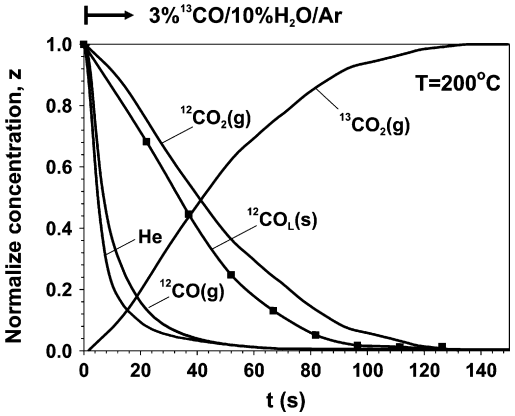

Fig. 8. Normalized concentration (Z) versus time transient response curves of ^{12}C-labeled gaseous CO and CO_2, and adsorbed linear CO species ($^{12}CO_L(s)$) found in the "C-path" of the WGS reaction at 200 °C on the 0.5 wt% Pt/TiO_2 catalyst. All transient response curves were recorded during *operando SSITKA* (DRIFTS–mass spectrometry) studies. The $^{13}CO_2(g)$ transient response curve is also shown to illustrate the accuracy of the SSITKA experiment performed.

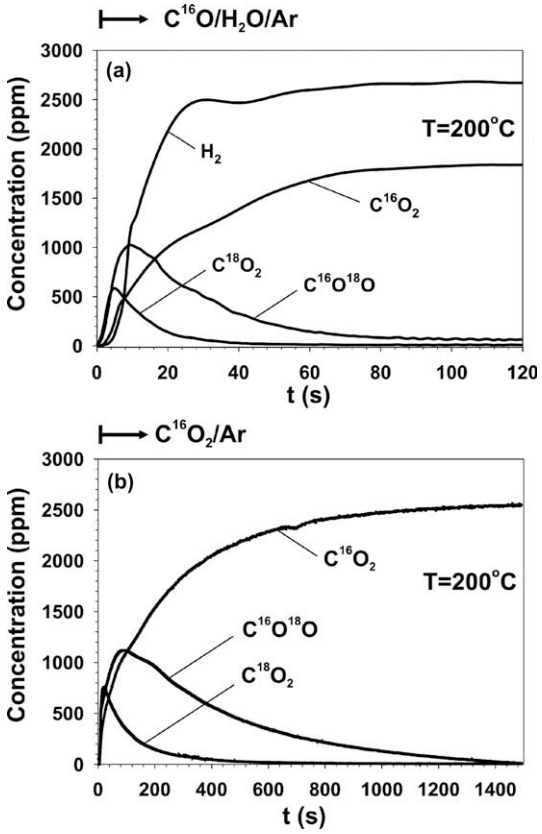

Fig. 9. (a) Transient response curves of H_2, $C^{16}O_2$, $C^{16}O^{18}O$, and $C^{18}O_2$ obtained during $^{18}O/^{16}O$ isotope exchange followed by WGS reaction at 200 °C (see Section 2.4.3) over the 0.5 wt% Pt/TiO_2 catalyst. (b) Transient response curves of isotopic carbon dioxides recorded at 200 °C under the 0.3%$C^{16}O_2$/Ar switch according to the gas delivery sequence: 5%$^{18}O_2$/He (600 °C, 30 min) → He, cool down to 80 °C → 1 atm H_2 (20 min, 80 °C) → He (20 min, 200 °C) → 0.3%$C^{16}O_2$/Ar (200 °C, t).

performed. Following exactly the same pre-treatment of the catalyst with $^{18}O_2$ and H_2 as described in Section 2.4.3, the catalyst was exposed at 200 °C to a 0.3%$C^{16}O_2$/Ar gas mixture and the transient evolution of all carbon dioxide isotopic species was followed with an *on-line* mass spectrometer. The obtained transient response curves are presented in Fig. 9b. It is clearly seen that the time evolution of all isotopic CO_2's lasts much longer (about 10 times, e.g. 120 vs. 1200 s) than that in the case presented in Fig. 9a (switch to the $C^{16}O/H_2O$/Ar mixture). In addition, while the maximum concentration of $C^{18}O^{16}O$ and $C^{18}O_2$ appears after 9.3 and 4.6 s, respectively from the switch to the WGS reaction mixture, similar maximum concentration values appear at much longer times, 86.2 and 19.8 s, respectively, from the switch to the $C^{16}O_2$/Ar gas mixture. It is rather clear that the two isotopic experiments presented in Fig. 9a and b strongly suggest that the kinetics of production of ^{18}O-containing carbon dioxide under WGS reaction conditions is much faster than the kinetics of simple exchange of the ^{16}O of gaseous CO_2 with the ^{18}O on the titania surface. It should also be noted that the concentration of 0.3 vol% CO_2 used in the CO_2/Ar feed (Fig. 9b) was similar to the CO_2 concentration formed under steady-state WGS reaction conditions for the same amount of catalyst used in the experiments presented in Fig. 9a and b. Furthermore, the same experiment that is presented in Fig. 9a when performed on the TiO_2 alone gave no production of any isotopic CO_2.

Any adsorbed ^{18}O on Pt during the 5%$^{18}O_2$/He (30 min, 600 °C) gas treatment was removed under the 1 atm H_2 (20 min, 80 °C) treatment as revealed by H_2-TPR experiments reported elsewhere [4]. Thus, the carbon dioxide isotopic responses shown in Fig. 9 refer to the titania support. Integration of the $C^{18}O^{16}O$ and $C^{18}O_2$ response curves based on the following material balance Eq. (7) provides the amount (μmol/g) of ^{18}O of titania support which participates in the corresponding chemical reaction processes.

$$N_{^{18}O}(\mu mol\,^{18}O/g_{cat}) = \left(\frac{F_T}{W}\right)\left[\int_0^t \left(2y_{C^{18}O_2} + y_{C^{16}O^{18}O}\right)dt\right] \quad (7)$$

In Eq. (7), y_i is the molar fraction (mol%) of the gaseous species i, F_T is the total molar flow rate (mol/s) at the reactor outlet, and W is the mass (g) of catalyst used. In the case presented in Fig. 9a (switch to the WGS reaction feed stream), the amount of ^{18}O was found to be 12.6 μmol$^{18}O/g_{cat}$ or 0.55 equivalent monolayers of surface Pt (θ_O = 0.55), whereas in the case presented in Fig. 9b (switch to the CO_2/Ar feed stream) the amount of ^{18}O was significantly larger, 185 μmol$^{18}O/g_{cat}$ or θ_O = 8.07.

4. Discussion

4.1. Kinetic aspects of the WGS reaction on 0.5 wt% Pt/TiO_2 catalyst

The experimental results and kinetic analysis performed in the present work revealed that the WGS reaction on the present 0.5 wt% Pt/TiO_2 catalyst is of 0.5, 1.0, ~0.0, and −0.7 order with respect to CO, H_2O, CO_2, and H_2, respectively. A large number of kinetic studies reported over noble metal supported catalysts refer to an almost zero reaction order with respect to CO [19,21,24,25,29,30]. For example, Hillaire et al. [25] reported that the reaction rate over Pd/CeO_2 is not affected by the CO partial pressure due to complete saturation of the Pd surface with CO, resulting in zero reaction order with respect to CO. This is also in accordance with the results of Azzam et al. [19] for the Pt–Re/TiO_2 catalytic system. On the other hand, the same group also reported that the reaction order with respect to CO depends on the range of CO concentration used in the feed stream. Although at high CO concentrations (3–12 vol%) the reaction rate was close to zero order, at lower CO concentrations (1–4 vol%) the reaction order with respect to CO takes positive values (0.4) comparable to the value of 0.5 estimated in the present work. Similarly, Jacobs et al. [12] found a zero-order dependency of reaction rate on CO over Pt/CeO_2 at high CO/H_2O molar ratios, whereas at low CO/H_2O molar ratios the reaction rate dependency on CO was found to be of first order; the surface coverage of adsorbed CO is influenced by the reaction rate. Moreover, Mhadeshwar et al. [22] found that over Pt-based catalysts the reaction order with respect to CO was −1.0 according to a micro-kinetic modeling that was performed. However, they observed that the coverage of adsorbed CO decreased with an increase in the reaction temperature. This led the authors to conclude that at higher reaction temperatures the reaction order with respect to CO is expected to be positive [22]. This is in agreement with the results of Jacobs et al. [12] for the Pt/CeO_2 catalyst who concluded that at high temperatures the surface coverage of CO is low, where the observed reaction order with respect to CO was 1.0.

The first-order dependency with respect to H_2O of the WGS reaction rate indicates that the latter increases in proportion with the partial pressure of H_2O (Fig. 1B). A first-order dependency of the WGS reaction rate has also been reported previously [19,24,28–30], and this was explained assuming that the rate is limited by the re-oxidation of support by water. This is likely to be the case for the present catalytic system, considering that the red-ox mechanism is valid as discussed next, according to which the CO molecule adsorbed on the Pt metal is oxidized by labile oxygen originating from the titania support, which in turn is re-oxidized by water. Ovesen et al. [28] have demonstrated over Cu-based catalysts that reaction orders with respect to reactants depend on the concentration of H_2O in the feed stream. In particular, for low H_2O feed concentrations the WGS reaction becomes first and zero order with respect to H_2O and CO, respectively, whereas by increasing the concentration of H_2O in the feed stream a progressive increase of the surface concentration of –OH groups occurs, leading to zero and first reaction orders, respectively, with respect to H_2O and CO. In a recent theoretical study [54] a water-mediated mechanism for the WGS reaction over a Rh cluster revealed that co-adsorbed water molecules can lower the free energy barrier of the rate-determining step (RDS) by 4.0 kcal/mol, thus providing a good explanation for the positive kinetic order of WGS with respect to H_2O. It is speculated whether this phenomenon could also apply to reduced titania sites offered for H_2O dissociation.

The negative reaction order (−0.7) with respect to H_2 (Fig. 2B) may be attributed to the competitive adsorption of $H_2$with CO. This explanation finds strong support from the present results of the *in situ* DRIFTS experiments (Fig. 5). It is clearly seen that in the case of CO/H_2 co-adsorption (Fig. 5, dashed line spectrum), the integral band area for the CO adsorbed species is dramatically decreased due to the presence of H_2 compared to the case of CO adsorption alone (absence of H_2, Fig. 5, solid line spectrum); the integral band area of CO is proportional to its surface concentration. Another possible explanation is that H_2 as a reaction product enhances the reverse WGS reaction, resulting in a decrease of the net reaction rate. The latter agrees also with the results reported by Hillaire et al. [25] on a Pd/CeO_2 catalyst, who attributed the −1.0 reaction order with respect to H_2 to the competitive adsorption of the latter with CO on Pd, or to the competition with H_2O for oxidation of the reduced ceria, or to the reversibility effect of the WGS reaction. Similarly, Phatak et al. [29] suggested that H_2 inhibition of the forward rate of WGS reaction is responsible for the negative reaction order (close to −0.5) with respect to H_2 over Pt/CeO_2 and Pt/Al_2O_3 catalysts. The authors proposed that atomic hydrogen is the dominant adsorbed surface species on the free Pt sites under CO equilibrium coverage conditions. A different explanation was given by

Azzam et al. [19] who proposed that hydrogen inhibits the WGS reaction rate over Pt/TiO_2 catalysts by suppressing the formation of OH groups on TiO_2 since the reaction step between adsorbed CO on Pt and OH groups of TiO_2 is the rate-determining step.

The zero order of WGS reaction with respect to CO_2 is a consequence of the fact that addition of CO_2 in the reaction feed (CO/H_2O) does not affect the rate-limiting step of the WGS, at least in the 210–270 °C range and for the feed compositions investigated (Fig. 2B). Azzam et al. [19] attributed the zero-order kinetics with respect to CO_2 to the fast desorption step of CO_2 on TiO_2. Similarly, Phatak et al. [29] found that the reaction order with respect to CO_2 on Pt/CeO_2 and Pt/Al_2O_3 catalysts is slightly negative and close to zero, respectively, due to the very weak interaction of CO_2 with Pt.

An apparent activation energy, E_a = 10.8 kcal/mol, was estimated for the various feed gas compositions depicted in Fig. 3. This is in agreement with the results of Hilaire et al. [25] who found that E_a = 9.1 kcal/mol for a Pd/CeO_2 catalyst and of Bunluesin et al. [24] who reported activation energies of 11 ± 1 kcal/mol for CeO_2-supported Pt, Rh, and Pd catalysts. A lower apparent activation energy (7.2 kcal/mol) was reported for Pt–Re/TiO_2 [19], while higher activation energies have been reported for Pt/Al_2O_3 (16.3 kcal/mol) [29], Pt/CeO_2 (17.9 kcal/mol) [29], $Cu/ZnO/Al_2O_3$ (13.2–20.6 kcal/mol) [26,27], and Fe-based (27.5 kcal/mol) catalysts [1].

4.2. Mechanistic aspects of the WGS reaction on 0.5 wt% Pt/TiO_2

The surface coverage of active "H-containing" reaction intermediates was found to be significantly larger than one (θ_H = 1.75, Fig. 6A), a result that strongly suggests that a significant concentration of these species resides on the surface of TiO_2. The chemical nature of these active "H-containing" intermediates is considered to be that of labile hydroxyls and atomic hydrogen (H), the latter attached on surface oxygen anions, O^{n-}, of the titania support and/or on the Pt surface. It has been suggested [19,20,55] that oxygen defect vacancies ($\square_s$) in partially reducible metal oxides such as titania can act as specific sites for H_2 activation. Evidence for the presence of such sites at the metal–support interface ([Pt-$\square_s$-Ti^{3+}] sites) is provided by the appearance of the LF-linear CO band that was previously discussed (1985 cm^{-1}, Fig. 5; 1995 cm^{-1}, Fig. 7C), where the presence of H_2 in the CO/H_2 gas adsorption mixture significantly reduced the coverage of this particular adsorbed CO species.

Oxygen vacancies on the support also contribute to the activation of water. It is therefore possible that the presence of hydrogen at these oxygen vacant sites (formation of Ti^{4+}–H^-) [55] hinders activation of H_2O, thus influencing the formation of OH-s and O-s (s = support site) according to the following reaction steps [9,19,20,25,55,56]:

$$\square_s + H_2O(g) \rightarrow O\text{-}s + H_2(g) \quad (8)$$

$$\square_s + H_2O(g) \rightarrow OH\text{-}s + 1/2H_2(g) \quad (9)$$

$$\square_s + H_2O(g) + O\text{-}s \rightarrow 2OH\text{-}s \quad (10)$$

The inhibiting effect of H_2 on the re-oxidation of reduced titania by H_2O (Eqs. (8) and (9)) could be another factor in explaining the negative reaction order with respect to H_2 besides that of lowering the surface concentration of adsorbed CO on [Pt-$\square_s$-Ti^{3+}] sites (Figs. 5 and 7C).

In what follows, the influence of reaction steps (8)–(10) and the adsorption of H on oxygen vacant sites of titania support on the estimation of "H-pool" size is discussed.

(a) Considering that atomic hydrogen is accommodated irreversibly on oxygen vacant sites forming Ti^{4+}–H^- species [55], where these oxygen vacant sites participate in reaction steps (8)–(10), then it is obvious that this kind of adsorbed H does not participate in the formation of H_2(g). It simply blocks active sites necessary for water activation or CO chemisorption, as previously discussed. On the other hand, if the hydrogen interaction is considered reversible, then the surface concentration of this kind of hydrogen species will be measured in the SSITKA experiment (Fig. 6A).

(b) If reaction step (9) is considered either irreversible or reversible, then since it is part of the "H-path" for hydrogen formation, the surface OH-s species involved is included in the "H-pool" reported in Section 3.3.1.

(c) If reaction step (8) is considered as an irreversible step, and since no adsorbed "H-containing" intermediate species are involved, this step does not participate in the measurement of "H-pool". On the other hand, if reaction step (8) is considered as an irreversible one, then the H_2(g) and HD(g) responses responsible for the measurement of "H-pool" have been underestimated, since formation of HDO(g) was not measured. In other words, the actual size of "H-pool" would be higher than what is reported in Section 3.3.1.

Based on the SSITKA–MS results presented in Fig. 6A, the rate of H_2 production appears to be larger than that of D_2 ($R_{H_2}/R_{D_2} > 2$). This implies the existence of a normal kinetic isotopic effect (KIE), where an elementary reaction step associated with the breaking or formation of a chemical bond that involves H can be considered. For example, surface diffusion of H species (breaking of O–H bond) and/or water dissociation on the titania surface could be considered as likely rate-determining elementary steps of the "H-path" of the WGS reaction as discussed next. It is also noted that due to the D-isotopic effect (Fig. 6A), the time required to reach the new steady state for the D_2(g) production is larger than that for the $^{13}CO_2$(g) production (Fig. 6B) during the SSITKA–MS experiment.

In contrast to the large concentration of "H-pool", the concentration of "C-pool" was found to be 0.007 of a monolayer (θ_C) at 200 °C, and θ_C = 0.18 at 250 °C for the present Pt/TiO_2 catalyst. These results may suggest that the active "carbon-containing" intermediates are associated only with the Pt metal surface or with peripheral sites at the metal–support interface. However, the possibility that all or part of it might be present on the support cannot be excluded.

SSITKA–DRIFTS results (Fig. 7A and B) clearly showed that formate species formed on the titania support surface must be considered as *inactive* (spectator) reaction intermediates since their characteristic IR bands (νCH and OCO vibrational modes) did not give the expected red isotopic shift. However, the presence of a very small concentration of potentially active formate species located at the metal–support interface cannot be excluded due to the experimental difficulty to resolve it by DRIFTS. It is worth noting that recent DRIFTS experimental results from our laboratory on the 0.5 wt% Pt/γ–Al_2O_3 catalyst showed that formate species did not decompose to CO_2 and H_2 at temperatures lower than 250 °C after adsorption of formic acid vapor at 25 °C followed by He TPD.

The results presented in Fig. 7C (upper graph) show that the IR bands centered at 2076, 2046, and 1995 cm^{-1} due to three kinds of linear adsorbed CO gave the red isotopic shift ($\Delta\nu$ = 52–54 cm^{-1}). Since CO is the only "carbon-containing" reactant species, it becomes clear that at least part of it must be considered to actively participate in the "carbon-path" of the WGS reaction.

It was found (Fig. 8, Section 3.3.2) that CO(g) produced during the SSITKA experiment under the present WGS reaction conditions (T = 200 °C) amounts to 23.0 μmol/g or θ = 0.95. Since only a very small amount of active "carbon-containing" species is populated under WGS reaction conditions (θ < 0.01, Section 3.3.1), it is clear that most of reversibly adsorbed CO populated on the Pt surface

(see Fig. 7C) is *inactive* toward the WGS reaction. The fact that the equivalent CO(g) produced during the aforementioned SSITKA experiment is relatively large, $\theta = 0.95$, some of this CO may not be justified as reversibly adsorbed CO on Pt. We have recently reported that on 0.5 wt% Pt/Al_2O_3 catalyst [33] adsorbed CO can reversibly interact with hydroxyl groups to form formate species according to the following reaction step:

$$CO\text{-}s + OH\text{-}s \leftrightarrow COOH\text{-}s + s \quad (11)$$

During the SSITKA experiment (gas switch to $^{13}CO/H_2O$), this kind of formate species even in case that it would be considered as a spectator species it will still decompose to give $^{12}CO(g)$, since CO-s interacts reversibly with gaseous CO, while at the same time the equivalent $^{13}COOH$-s will be formed. Given the fact that it was impossible to resolve in Fig. 7A and B any very small IR band of formate giving the red isotopic shift, only a very small quantity of such formate species might have been formed according to reaction step (11).

According to the reaction mechanisms proposed in the literature [3,7,8,12,17,18,33], two different carbon-paths from the reactant CO to the product CO_2 are considered:

$$Pt{-}CO + OH\text{-}s \rightarrow CO_2(g) + 1/2H_2(g) + \square_s + Pt \quad (12)$$

$$Pt{-}CO + O\text{-}s \rightarrow CO_2(g) + \square_s + Pt \quad (13)$$

The first step (Eq. (12)) is part of the associative mechanism of the overall WGS reaction proposed in the literature. It has been suggested that the WGS reaction proceeds via formate or carbonate active intermediate species, the former produced by the interaction of CO adsorbed on platinum with a hydroxyl group of TiO_2 at the metal–support interface. Following an earlier work by Shido and Iwasawa [13], Jacobs et al. [12,18,46,47] proposed that formate generated by the reaction of CO with a bridging OH group associated with Ce^{3+} defect site (CeO_{2-x} support) was the main reaction intermediate. Recently, Meunier et al. [57] proposed that formates can potentially be active intermediates on Pt/CeO_2 above 200 °C, whereas the same species as observed by DRIFTS were merely reaction spectators below this temperature.

The production of $C^{18}O^{16}O$ and $C^{18}O_2$ isotopic gaseous species observed after pre-treatment of the catalyst with $^{18}O_2$ followed by H_2 treatment and a switch to the WGS reaction stream (Fig. 9a) strongly favours the participation of lattice oxygen of the titania support in the WGS reaction mechanism also according to the results (Fig. 9b) and remarks presented in the previous Section 3.3.3. It is also important to note that after performing the same experiment but using a 3%^{12}CO/Ar instead of 3%^{12}CO/10%H_2O/Ar gas mixture (Fig. 9a) or $^{12}CO_2$/Ar (Fig. 9b) in the last step of the sequence of step gas switches which was followed, the amount of $C^{18}O^{16}O$ and $C^{18}O_2$ obtained was 4.0 μmol ^{18}O/g ($\theta_O = 0.18$), which is about one-third of that observed under WGS reaction conditions. Furthermore, similar shapes and positions in time for the transient curves of $C^{16}O^{18}O$ and $C^{18}O_2$ were recorded. The latter result is an additional strong evidence in favour of a *red-ox* mechanism operated on the present Pt/TiO_2 catalyst as depicted by reaction steps (8)–(10), (12), and (13).

The switch Ar (200 °C) → $C^{16}O/H_2O$/Ar (200 °C, t) corresponds to an ordinary transient experiment (step gas concentration change), where the transient rates of H_2 and CO_2 production (Fig. 9a) may not be the same as ought to be under steady-state WGS reaction conditions. In other words, during the transient period the "H-path" does not have the same rate as the "C-path". Therefore, the small delay observed in the H_2 response with respect to the $C^{16}O_2$ response shown in Fig. 9a can be understood, and there is no reason to invoke that this might be caused by any H_2 re-adsorption effect. The fact that the rate of H_2 production is larger than that of $C^{16}O_2$ after 120 s of the switch to the WGS reaction feed stream is due to the irreversible formation of carbonates which is in harmony with the SSITKA–DRIFTS results shown in Fig. 7A. After a longer time on stream the concentrations of H_2 and CO_2 become the same.

The fact that the labeled CO_2's appear first compared to the $C^{16}O_2$ as shown in Fig. 9a is related to the relative magnitude of the transient rate of $C^{16}O^{18}O$ production via the interaction of gaseous $C^{16}O$ and pre-adsorbed surface ^{18}O, and to that of $C^{16}O_2$ production via the WGS reaction. The fact that the transient formation of $C^{18}O_2$ appears in a significantly shorter time as compared to the case of simple CO_2 exchange (Fig. 9b) and with similar maximum rate seems to imply that under WGS reaction conditions the binding energy of given surface oxygen species is reduced. Furthermore, considering that $C^{18}O_2$ can only be formed via the interaction of $C^{16}O^{18}O$ with ^{18}O on the surface, it implies that the actual initial $C^{16}O^{18}O$ concentration formed via the *red-ox mechanism* of the WGS reaction is larger by the equivalent amount of $C^{18}O_2$ formed, implying that the estimated amount of the active ^{18}O that participates in the red-ox mechanism of the WGS reaction is correct ($\theta_O = 0.55$).

Based on the discussion offered above, it is suggested that the WGS reaction over the present 0.5 wt% Pt/TiO_2 catalyst at 200 °C follows a *red-ox mechanism*, where CO adsorbs on Pt and reacts at the metal–support interface with labile oxygen present at the Pt–titania support interface, thus forming CO_2 (see Eq. (12)). On the contrary, Azzam at al. [19,20] proposed an associative mechanism with red-ox regeneration over titania-supported catalysts based on FTIR studies that showed the presence of formates on titania under WGS reaction conditions. However, the authors did not provide any experimental evidence whether the formate species observed should be convincingly considered as *active* reaction intermediates, thus excluding or not the red-ox mechanism (no SSITKA–DRIFTS studies were performed).

A schematic presentation of the proposed *red-ox* mechanism of the WGS reaction over the present 0.5 wt% Pt/TiO_2 catalyst, also incorporating the isotopic results presented in Fig. 9a, is shown in Scheme 1. Gaseous CO is adsorbed on Pt present within atomic distance from the O atom of the titania support (metal–support interface), labeled as ^{18}O, which then is in energetically favorable position to react with labile ^{18}O to form $C^{16}O^{18}O(g)$. The reduced titania formed is then re-oxidized by H_2O to release $H_2(g)$ according to the elementary reaction steps 8 and 9. The OH_{ad} formed (step 9) is subsequently dissociated into H_{ad} and O_{ad} [9], and $H_2(g)$ is formed on the Pt surface. Calatayud et al. [58] have also presented evidence that the surface of TiO_2 can be reduced by CO and oxidized by H_2O.

4.3. Some remarks on the operando-DRIFTS–mass spectrometry studies

In Fig. 8 it is clearly seen that the $^{12}CO_L(s)$ transient response curve lags behind that of $^{12}CO(g)$ since the latter species is a pre-

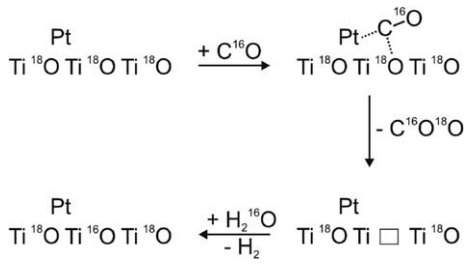

Scheme 1. Proposed elementary reaction steps of the WGS reaction over the 0.5 wt% Pt/TiO_2 catalyst after $^{16}O/^{18}O$ exchange followed by $C^{16}O/H_2{}^{16}O$ WGS reaction ($T = 200$ °C).

cursor intermediate responsible for the formation of adsorbed $CO_L(s)$. The latter species in turn is responsible for the formation of $^{12}CO_2(g)$ via a *red-ox* path [$CO(g) \rightarrow CO_L(s) \rightarrow CO_2(g)$]. The dynamics of depletion of $^{12}CO_L(s)$ upon the isotopic switch ($^{13}CO/H_2O$) will depend both on the size (concentration of adsorbed $^{12}CO_L$) and on the kinetics of the elementary reaction steps (Eqs. (12) and (13)). For example, it will depend on the rate constants, *k*'s, and surface concentrations of OH-s and O-s active intermediates. The elementary steps 12 and 13 to occur may require surface diffusion of adsorbed CO_L from Pt to the metal–support interface in order to reach labile O-s/OH-s of the titania support.

On the other hand, the fact that a red isotopic shift was observed for this specific $CO_L(s)$ adsorbed species (2046 cm^{-1}, Fig. 7C) does not necessarily mean that this is a true active reaction intermediate. The dynamics of $^{12}CO_L(s)$ observed (Fig. 8) could alternatively be interpreted as due only or partly to the kinetics of isotopic exchange of $^{12}CO(g)$ with $^{12}CO_L(s)$. To resolve this issue one has to measure the rate of isotopic exchange under reaction conditions and compare it with the measured rate of reaction. Such investigation was out of the scope of the present work.

In Fig. 7C it is obvious that all the three $CO_L(s)$ species that were identified (2076, 2046, and 1995 cm^{-1}) gave the red isotopic shift. According to what is mentioned in the previous paragraph, these $CO_L(s)$ adsorbed species may not be all true active intermediates of the WGS reaction. For the present catalytic system, deconvolution of the spectrum was necessary (Fig. 7C) in order to follow an accurate estimation of the area change under each deconvoluted band with time during the isotopic switch. This information could be used in conjuction to the results presented in Fig. 8 to check whether the transient response curves of the other two $CO_L(s)$ species (2076, 1995 cm^{-1}, Fig. 7C) are placed below or above the $^{12}CO_2(g)$ transient response curve. In the latter case, it is clear that this specific $CO_L(s)$ species cannot be an active intermediate, whereas in the former case it could be considered as an active intermediate. Due to the low intensities recorded for these two $CO_L(s)$ species under a steady state (Fig. 7C), it is obvious that after the isotopic switch these intensities would have become even lower (depletion of adsorbed $^{12}CO_L(s)$). Therefore, this methodology cannot be applied for low-intensity IR bands associated with reversibly adsorbed reaction intermediates.

Finally, the $^{12}CO_2(g)$ transient response curve lags behind that of $CO_L(s)$ since the $CO_2(g)$ is considered to be the final product of the "carbon-path" of the WGS reaction. For very fast reaction steps 12 and 13, and assuming no re-adsorption of $CO_2(g)$, the $^{12}CO_L$ and $^{12}CO_2(g)$ transient response curves ought to coincide, which is not the case (Fig. 8). As discussed in the Result Section 3.3.2, the correct appearance of $^{13}CO_2(g)$ transient response curve relative to its counterpart of $^{12}CO_2(g)$ confirms the validity of the accuracy of the present SSITKA-operando studies.

5. Conclusions

The following conclusions can be considered from the results of the present work:

(a) The kinetic rate of the WGS reaction in the 210–270 °C range over the present 0.5 wt% Pt/TiO_2 catalyst increases with an increase in the concentration of CO or H_2O in the feed stream, while the opposite is true for the case of H_2. On the other hand, the rate of reaction does not practically depend on the concentration of CO_2 in the feed stream.

(b) The experimental kinetic reaction rate measurements that were obtained were fitted very well to an empirical power-law rate expression, according to which the WGS reaction is 0.5, 1.0, zero, and −0.7 order with respect to CO, H_2O, CO_2, and H_2, respectively. The apparent activation energy of the reaction was found to be 10.8 kcal/mol.

(c) Based on detailed SSITKA–DRIFTS, SSITKA–MS, and other transient ^{18}O-isotopic exchange experiments, it is strongly suggested that the WGS reaction on the present 0.5 wt% Pt/TiO_2 catalyst passes through a *red-ox mechanism*, where CO adsorbs on Pt, diffuses toward the metal–support interface, and then reacts with labile oxygen of the titania support at the metal–support interface to form CO_2.

(d) Two kinds of formate species, and carbonate adsorbed species that formed on the TiO_2 support surface observed by SSITKA–DRIFTS experiments are considered as *inactive* or *spectator species* of the steady-state WGS reaction.

(e) Only a very small surface coverage ($\theta < 0.1$) of adsorbed CO on the Pt surface participates in the reaction mechanism of the WGS reaction on the present 0.5 wt% Pt/TiO_2 catalyst.

Acknowledgments

This work was funded by the Research Committee of the University of Cyprus, the General Secretariat of Research and Technology (GSRT) Hellas, and the Commission of the European Community under the PENED 2001 Program (contract 01ED561).

References

[1] D.S. Newsome, Catal. Rev. Sci. Eng. 21 (1980) 275.
[2] A.F. Ghenciu, Curr. Opin. Solid State Mater. Sci. 6 (2002) 389.
[3] D.L. Trimm, Z.I. Önsan, Catal. Rev. 43 (2001) 31.
[4] P. Panagiotopoulou, A. Christodoulakis, D.I. Kondarides, S. Boghosian, J. Catal. 240 (2006) 114. and references therein.
[5] P. Panagiotopoulou, D.I. Kondarides, J. Catal. 225 (2004) 327. and references therein.
[6] P. Panagiotopoulou, D.I. Kondarides, Catal. Today 112 (2006) 49.
[7] J. Barbier, D. Duprez, Appl. Catal. B 3 (1993) 62.
[8] Y. Choi, H.G. Stenger, J. Power Sources 124 (2003) 432.
[9] R.J. Gorte, S. Zhao, Catal. Today 104 (2005) 18.
[10] X. Wang, R.J. Gorte, J.P. Wagner, J. Catal. 212 (2002) 225.
[11] G. Jacobs, P.M. Patterson, U.M. Graham, A.C. Crawford, B.H. Davis, Int. J. Hydrogen Energy 30 (2005) 1265.
[12] G. Jacobs, L. Williams, U. Graham, G.A. Thomas, D.E. Sparks, B.H. Davis, Appl. Catal. A: Gen. 252 (2003) 107.
[13] T. Shido, Y. Iwasawa, J. Catal. 141 (1993) 71.
[14] A.M. Efstathiou, X.E. Verykios, Appl. Catal. A: Gen. 151 (1997) 109. and references therein.
[15] D. Tibiletti, A. Goguet, D. Reid, F.C. Meunier, R. Burch, Catal. Today 113 (2006) 94.
[16] A. Goguet, F.C. Meunier, D. Tibiletti, J.P. Breen, R. Burch, J. Phys. Chem. B 108 (2004) 20240.
[17] G. Jacobs, A.C. Crawford, B.H. Davis, Catal. Lett. 100 (2005) 147.
[18] G. Jacobs, B. Davis, Appl. Catal. A 284 (2005) 31.
[19] K.G. Azzam, I.V. Babich, K. Seshan, L. Leffers, Appl. Catal. B: Environ. 80 (2008) 129.
[20] K.G. Azzam, I.V. Babich, K. Seshan, L. Lefferts, J. Catal. 251 (2007) 153.
[21] D.C. Grenoble, M.M. Estadt, D.F. Ollis, J. Catal. 67 (1981) 90.
[22] A.B. Mhadeshwar, D.G. Vlachos, Catal. Today 105 (2005) 162.
[23] C. Wheeler, A. Jhalani, E.J. Klein, S. Tummala, L.D. Schmidt, J. Catal. 223 (2004) 191.
[24] T. Bunluesin, R.J. Gorte, G.W. Graham, Appl. Catal. B 15 (1998) 107.
[25] S. Hilaire, X. Wang, T. Luo, R.J. Corte, J. Wagner, Appl. Catal. A 215 (2001) 271.
[26] N.A. Koryabkina, A.A. Phatak, W.F. Ruettinger, R.J. Farrauto, F.H. Ribeiro, J. Catal. 217 (2003) 233.
[27] C.V. Ovesen, B.S. Clausen, B.S. Hammershøi, G. Steffensen, T. Askgaard, I. Chorkendorff, J.K. Norskov, P.B. Rasmussen, P. Stolze, P. Taylor, J. Catal. 158 (1996) 170.
[28] C.V. Ovesen, P. Stoltze, J.K. Nørskov, C.T. Campbell, J. Catal. 134 (1992) 445.
[29] A.A. Phatak, N. Koryabkina, S. Rai, J.L. Ratts, W. Ruettinger, R.J. Farrauto, G.E. Blau, W.N. Delgass, F.H. Ribeiro, Catal. Today 123 (2007) 224.
[30] R. Radhakrishnan, Z.D.R.R. Willigan, Z. Dardas, T.H. Vanderspurt, Appl. Catal. B: Environ. 66 (2006) 23.
[31] K. Polychronopoulou, C.N. Costa, A.M. Efstathiou, Appl. Catal. A: Gen. 272 (2004) 37.

[32] G.G. Olympiou, C.M. Kalamarasa, C.D. Zeinalipour-Yazdia, A.M. Efstathiou, Catal. Today 127 (2007) 304.
[33] C.M. Kalamaras, G.G. Olympiou, A.M. Efstathiou, Catal. Today 138 (2008) 228.
[34] B.C. Smith, Fundamentals of Fourier Transform Infrared Spectroscopy, CRC Press, 1996.
[35] J. Sirita, S. Phanichphant, F.C. Meunier, Anal. Chem. 79 (2007) 3912.
[36] P. Panagiotopoulou, D.I. Kondarides, J. Catal. 260 (2008) 141.
[37] O.S. Alexeev, S.Y. Chin, M.H. Engelhard, L. Ortiz-Soto, M.D. Amiridis, J. Phys. Chem. B 109 (2005) 23430.
[38] F. Boccuzzi, A. Chiorino, M. Manzoli, D. Andreeva, T. Tabakova, J. Catal. 188 (1999) 176.
[39] A. Yee, S.J. Morrison, Hicham Idriss, J. Catal. 191 (2000) 30.
[40] P. Panagiotopoulou, J. Papavasiliou, G. Avgouropoulos, T. Ioannides, D.I. Kondarides, Chem. Eng. J. 134 (2007) 16.
[41] A. Bensalem, J.C. Muller, D. Tessier, F. Bozon-Verduraz, J. Chem. Soc. Faraday Trans. 92 (1996) 3233.
[42] P. Winslow, A.T. Bell, J. Catal. 86 (1984) 158.
[43] U. Diebold, Surf. Sci. Rep. 48 (2003) 53.
[44] K.D. Schierbaum, S. Fischer, M.C. Torquemada, J.L. de Segovia, E. Román, J. Martín Gago, Surf. Sci. 345 (1996) 261.
[45] G. Busca, J. Lamotte, J.-C. Lavalley, V. Lorenzelli, J. Am. Chem. Soc. 109 (1987) 5197. and references therein.
[46] G. Jacobs, A. Crawford, L. Williams, P.M. Patterson, B.H. Davis, Appl. Catal. A: Gen. 267 (2004) 27.
[47] G. Jacobs, S. Khalid, P.M. Patterson, L. Williams, D. Sparks, B.H. Davi, Appl. Catal. A:Gen. 268 (2004) 255.
[48] K. Almusaiter, S.S.C. Chuang, J. Catal. 180 (1998) 161.
[49] A.M. Bradshaw, H. Hoffman, Surf. Sci. 72 (1978) 513.
[50] D. Tessier, A. Rakai, F. Bonzon-Verduraz, J. Chem. Soc. Faraday Trans. 88 (1992) 741.
[51] T. Kecskés, J. Raskó, J. Kiss, Appl. Catal. A: Gen. 268 (2004) 9.
[52] K. Tanaka, J.M. White, J. Catal. 79 (1983) 81.
[53] G.S. Lane, E.E. Wolf, J. Catal. 105 (1987) 386.
[54] C.D. Zeinalipour-Yazdi, A.M. Efstathiou, J. Phys. Chem. C 112 (2008) 19030.
[55] M. Menetrey, A. Markovits, C. Minot, Surf. Sci. 524 (2003) 49.
[56] S. Hilaire, X. Wang, T. Luo, R.J. Gorte, J. Wagner, Appl. Catal. A: Gen. 258 (2004) 271.
[57] F.C. Meunier, D. Tibiletti, A. Goguet, S. Shekhtman, C. Hardacre, R. Burch, Catal. Today 126 (2007) 143.
[58] M. Calatayud, A. Markovits, M. Menetrey, B. Mguig, C. Mino, Catal. Today 85 (2003) 125.